Preliminary communication / Communication

# $^{19}F/^{29}Si$ distance determination and heteronuclear spin counting under fast magic-angle spinning in fluoride-containing octadecasil

Philippe Bertani, Jésus Raya, Jérôme Hirschinger *

*Institut de chimie, FRE 2446 CNRS, université Louis-Pasteur, BP 296, 67008 Strasbourg cedex, France*

## Abstract

$^{19}F/^{29}Si$ rotational-echo double-resonance (REDOR), $\theta$-REDOR and Hartmann–Hahn cross-polarization (CP) NMR techniques have been applied under fast magic-angle spinning (MAS) to a powder sample of fluoride-containing octadecasil. The internuclear distance of the $^{19}F–^{29}Si$ spin pairs formed by the silicons in the D4R units (T-1 site) and the fluoride anions deduced directly from the CP and REDOR measurements is in very good agreement with the X-ray crystal structure. Moreover, heteronuclear spin-counting $\theta$-REDOR experiments unambiguously show that the $^{19}F$ and the T-1 $^{29}Si$ nuclei form fairly isolated spin pairs, whereas multiple-spin behaviour is clearly evidenced at the T-2 site. *To cite this article: P. Bertani et al., C. R. Chimie 7 (2004).*

## Résumé

Les méthodes REDOR, $\theta$-REDOR et de polarisation croisée (CP) de type Hartmann–Hahn ont été appliquées en rotation rapide à l'angle magique à un échantillon de poudre de cathrasil octadecasil. La distance $^{19}F–^{29}Si$ obtenue directement des mesures REDOR et CP pour les atomes de silicium en site T-1 est en excellent accord avec les précédentes déterminations par diffraction des rayons X. En outre, des expériences de comptage de spin hétéronucléaire démontrent que les atomes de fluor et de silicium T-1 forment des paires quasiment isolées, alors que des interactions dipolaires multiples sont clairement mises en évidence au niveau des sites T-2. *Pour citer cet article : P. Bertani et al., C. R. Chimie 7 (2004).*

## 1. Introduction

Several nuclear magnetic resonance (NMR) techniques have been developed recently for the accurate measurement of internuclear distances. Many of these methods are designed to reintroduce dipolar couplings during magic-angle spinning (MAS) in order to exploit the recoupled dipolar interactions for the determination of molecular geometry, without sacrificing the good sensitivity and resolution provided by MAS. Hartmann–Hahn cross-polarization (CP) [1–3], in con-

---

* Corresponding author.

*E-mail address:* hirschinger@chimie.u-strasbg.fr
(J. Hirschinger).

junction with MAS, has been widely applied in high-resolution solid-state NMR studies [4–7]. Although the CP technique has been originally developed to overcome the problem of low sensitivity of rare spins *S* with low gyromagnetic ratios in solids containing also abundant spins *I*, it has long been recognized that the so-called transient oscillations of the CP dynamics generally observed for strongly coupled *IS* spin pairs contain valuable structural information through the determination of the heteronuclear dipolar coupling constant $D_{IS} = \mu_0 \gamma_S \gamma_I \gamma_S / (4 \pi r^3)$[5,8]. For static samples and continuous-wave cross-polarization (CWCP), it is well known that efficient polarization transfer through heteronuclear zero quantum (flip-flop) transitions is obtained at the Hartmann–Hahn matching condition $\omega_{1I} = \omega_{1S}$, where $\omega_{1I}$ and $\omega_{1S}$ are the amplitudes of the radiofrequency (RF) fields applied to the *I* and *S* spins [1,5]. When the spinning frequency $\omega_r$ exceeds both the *I–I* and *I–S* dipolar interactions, the single Hartmann condition splits into a series of new 'sideband' matching conditions $\Delta = \omega_{1I} - \omega_{1S} = n \omega_r$ and efficient CP is obtained only at the first- and second-order sidebands ($n = \pm1, \pm2$) [9,10]. At the $n = \pm1$ and $\pm2$ matching conditions, a secular (time-independent) flip-flop term exists because of the destructive interference between the modulation of the dipolar coupling by MAS and the RF fields. CWCP on a sideband matching condition may then be regarded as rotating-frame heteronuclear dipolar-recoupling technique. On the other hand, it has been suggested that dipolar recoupling may be achieved by the application of rotor-synchronized π pulses. Experiments of this kind form the basis of the established rotational-echo double-resonance (REDOR) technique introduced by Schaefer et al [11,12]. Although REDOR sequences are in principle plagued at high spinning speed by artefacts due to the finite π pulse lengths, it was demonstrated recently that REDOR functions quite satisfactorily under fast MAS conditions [13]. Numerous applications and extensions of REDOR have appeared [14–24].

In this paper, we report Hartmann–Hahn CWCP, REDOR and θ-REDOR NMR experiments under fast MAS in fluoride-containing octadecasil, which is an excellent model compound to test the reliability of dipolar recoupling methods [18,25–27]. After a presentation of the basic theory of the spin dynamics in (θ-)REDOR and Hartmann–Hahn CWCP (section 2),

experimental results are compared with analytical and numerical calculations.

## 2. Theory

### 2.1. Rotational-echo double-resonance

In a magic-angle spinning (MAS) experiment, the heteronuclear dipolar Hamiltonian for an isolated *S–I* spin pair is written as [5,28] (Eq. (1)):

$$H = 2 b(t) I_z S_z \tag{1}$$

where:

$$b(t) = \frac{D_{IS}}{2}\{\sqrt{2} \sin 2\beta \cos (\gamma + \omega_r t) \\ - \sin^2\beta \cos (2\gamma + 2\omega_r t)\} \tag{2}$$

($\alpha$, $\beta$, $\gamma$) are the Euler angles as defined by Spiess [28] relating the principal axes system (PAS) of the dipolar interaction tensor to the rotor fixed frame (ROT) (the angle $\alpha$ is absent from Eq. (2) due to the axial symmetry of the dipolar interaction). Eq. (2) shows that the average value of the dipolar interaction over each rotor cycle is zero, i.e., the dipolar coupling is re-focussed at the times of rotational echoes $N_c T_r$, where $N_c$ is the number of rotor periods ($T_r = 2 \pi/\omega_r$). In the REDOR experiment, rotational echo formation is prevented by applying rotor-synchronized π pulses. If π pulses are applied at every rotor half-cycle, the sign of the apparent Hamiltonian during the second half of each rotor period is opposite to that during the first half. Since this effective coupling operates for a time $N_c T_r$, the net dipolar-dephasing angle, $\varphi$, after $N_c$ rotor cycles is readily obtained:

$$\varphi = N_c \left[ \int_0^{T/2} b(t) \, dt - \int_{T/2}^{T_r} b(t) \, dt \right] \tag{3}$$

Using Eq. (2), the evaluation of Eq. (3) yields the well-known expression of the ratio of the observable *S*-spin signal with and without the π pulses [11,12,19,29,30]

$$\frac{S(\beta, \gamma)}{S_0} = \cos \varphi = \cos ( 2\sqrt{2} \, D \, N_c \, T_r \, \sin 2\beta \, \sin \gamma ) \tag{4}$$

where $D = D_{IS}/2\pi$ is the heteronuclear dipolar coupling constant in Hz.

After powder averaging of Eq. (4), one obtains a 'universal' REDOR dephasing curve $S/S_0$ as a function of the dimensionless parameter $\lambda = N_c\,T_r\,D$ that applies to all heteronuclear spin pairs [29,30] and the Fourier transform of this REDOR dephasing curve yields the so-called Pake-spun powder spectrum, whose separation between edges (in Hz) is equal to $2D\sqrt{2}/\pi$ [12].

### 2.2. Hartmann–Hahn cross-polarization

By transforming to the rotating frame of the nearest-resonant Fourier component of the time-dependent dipolar coupling $b(t)$ and applying 0th-order average Hamiltonian theory ($\omega_r >> D_{IS}$), one finds that the transferred polarization $M_S(t)$ evolves in the Hartmann–Hahn cross-polarization experiment as [31]:

$$\frac{M_S(t)}{M_S^{eq}} = \frac{\gamma_I}{2\gamma_S} \frac{\delta_n^2}{(\Delta - n\,\omega_r)^2 + \delta_n^2} \left[ 1 - \cos(\omega_e^{(n)}t) \right] \quad (5)$$

where $\omega_e^{(n)} = \sqrt{(\Delta - n\,\omega_r)^2 + \delta_n^2}$, $M_S^{eq}$ is the $S$-spin magnetization at thermal equilibrium in the static magnetic field $\mathbf{B}_0$, and the dipolar coupling elements are defined by:

$$\delta_{\pm 1} = \frac{D_{IS}}{4}\sqrt{2}\,\sin 2\beta \quad (6)$$

$$\delta_{\pm 2} = \frac{D_{IS}}{4}\,\sin^2\beta \quad (7)$$

At the $n = \pm 1$ and $\pm 2$ sideband matching conditions, Eq. (5) becomes (8):

$$\frac{M_S(t)}{M_S^{eq}} = \frac{\gamma_I}{2\gamma_S}\left[ 1 - \cos(\delta_n t) \right] \quad (8)$$

As in the static case, the dipolar coupling $D$ can directly be determined from the well-defined horns of Pake-like powder patterns [26,32,33]. In other words, at the first- and second-order matching conditions, recoupling of the heteronuclear interaction takes place. For $n = \pm 1$, the splitting in the powder pattern is found for $\beta = \pi/4$, and is smaller by a factor $\sqrt{2}$ than the splitting between the intense singularities in a Pake pattern ($S_{\pm 1} = D/\sqrt{2}$). For $n = \pm 2$, the maximum splitting is found for $\beta = \pi/2$, and is half that of the splitting in a Pake pattern for the same orientation

($S_{\pm 2} = D/2$). Hence, the $n = \pm 1$ matching condition is in principle preferred because of its larger recoupling efficiency. Note that the $n = \pm 1$ and $\pm 2$ lineshapes qualitatively differ from the Pake-spun powder pattern observed in the REDOR experiment because they only depend on the Euler angle $\beta$ (Eqs. (6) and (7)) and not on $\gamma$. In this case, the recoupled heteronuclear interactions are '$\gamma$ encoded' [34], indicating favourable performance in a powder. Indeed, this simplified angular dependence leads to a more pronounced time-domain oscillatory behaviour for long mixing time than for the REDOR dipolar-dephasing curve and gives rise to the characteristic divergences of the Pake doublet whose splitting $S_n$ with $n = \pm 1$ and $\pm 2$ is directly related to the dipolar coupling constant $D$.

## 3. Experimental

The NMR experiments were performed at room temperature on a Bruker Avance DSX-500 spectrometer, operating at frequencies of 99.33 and 470.48 MHz for $^{29}$Si and $^{19}$F resonance, respectively, and equipped with a Bruker $^{19}$F/X CP-MAS probe using a 4-mm o.d. rotor. The octadecasil sample was synthesized by Dr. E. Klock from LMM, Mulhouse, France. The powder sample was packed into a full MAS rotor (sample is ~15 mm long) or was restricted to a small volume (3.5-mm layer) in the centre of the coil to reduce RF field inhomogeneities [35] (hereafter called 'CRAMPS rotor' [36]). However, although the REDOR and Hartmann–Hahn CP experiments are in principle sensitive to pulse imperfections, no significant difference was observed between experiments performed with the different-sized samples. This result is attributed to the standard Hartmann–Hahn (HH) continuous wave cross-polarization ($n = \pm 1$ HH CP condition) step, which acts as an RF field amplitude filter [26]. In all the REDOR experiments, the observed nucleus was $^{29}$Si, and the trains of rotor-synchronous dephasing π-pulses were applied to $^{19}$F. The HH CP contact time before REDOR dephasing ranged from 15 to 30 ms and the recycle time from 5 to 10 s. No thermal problems in the sample or in the probe (detuning) caused by the rather long CP contact time were observed. $^{1}$H decoupling was not applied and it was observed that no gain in resolution was obtained by applying $^{19}$F decoupling during acquisition, thereby confirming that hetero-

nuclear interactions are efficiently suppressed by fast MAS. The $^{19}$F and $^{29}$Si RF fields were calibrated directly with the octadecasil sample using a two-dimensional nutation experiment [37]. The CP dynamics were obtained by measuring the integrated peak intensity in the silicon spectrum as a function of the contact time *t*. The time-domain REDOR signal is generated by increasing the number of rotor cycles in an experiment and observing the $^{29}$Si signal with and without the application of rotor-synchronized $^{19}$F dipolar-dephasing pulses to obtain a *reduced* (*S*) and a *full* signal ($S_0$), respectively [29]. The ratio $(S_0 - S)/S_0$ or $S/S_0$, which is independent of the relaxation time $T_2$ is then plotted as a function of time. The spin-counting $\theta$-REDOR experiments were performed by recording the variation of the echo amplitude, $S(\theta)$, as a function of the mid-pulse sequence flip angle $\theta$ at a given dephasing time $t_d$ [38]. Seven to 13 values of $\theta$ between 0 and $\pi$ were employed. Note that, in this case, there is no need for referencing, since the number of rotor cycles is held constant and $\theta$ is varied. Spin-counting stick spectra were generated by fitting $S(\theta)$ with a Fourier series verifying the conditions $S(0) = 1$ (for normalization) and $S(\pi) = 0$ (for baseline correction) [38]. In practice, only the first eight Fourier coefficients were meaningful.

## 4. Results and discussion

Fig. 1 shows a portion of the octadecasil framework showing the four D4R units surrounding each T-2 sili-
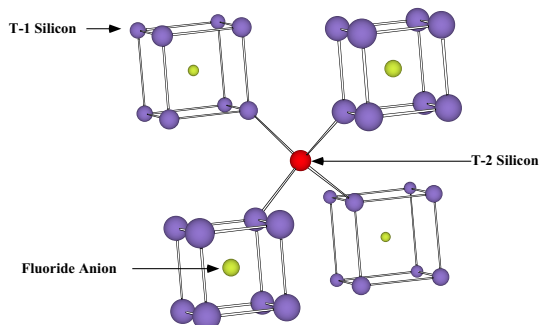


Fig. 1. Representation of a portion of the octadecasil framework showing the four 'Si$_8$-cubes' (D4R units) surrounding each T-2 silicon. The oxygen atoms (not shown) lie approximately at the midpoint of each line. Silicons in site 1 are connected to three other T-1 sites in the same D4R unit and one T-2 silicon. Each T-2 site links T-1 silicons from four different D4R units.

cons. Each T-2 site links T-1 silicons from different D4R units. The location of the fluoride anion in the centre of a D4R unit of eight silicons provides a good test case for distance determination by solid-state NMR methods since the low abundance of $^{29}$Si means that the dipolar interactions between the $^{19}$F and T-1 silicons are close to isolated spin pairs. Indeed, from the X-ray crystal structure, the T-1 silicons are 2.63 Å from the fluoride ion inside their D4R unit and more than 7 Å from the fluoride ions in adjacent D4R units while the closest F–F distance is 9.33 Å (Fig. 1).

Fig. 2 shows the experimental REDOR results for the $^{29}$Si in the T-1 site. The experimental data are well accounted for by calculations for an isolated $^{19}$F–$^{29}$Si spin pair with *D* between 1150 and 1200 Hz, i.e., with $r = 2.67 \pm 0.02$ Å (Fig. 2a). It is of interest to analyse the REDOR data in the frequency domain. The Fourier transform of the REDOR dephasing curve yields the so-called Pake-spun powder spectrum [12] (Fig. 2b) whose separation between edges (in Hz) is equal to $2D\sqrt{2}/\pi$. Since there is a large error in determining the position of a broadened edge, we have represented in Fig. 2c the power spectrum of the derivative of the lineshape of Fig. 2b. The dipolar coupling constant *D* can then be deduced *directly* from the line splitting of 1.1 kHz between the intense peaks of Fig. 2c. The corresponding value $D = 1.2$ kHz yields a Si–F distance $r \approx 2.65$ Å, in very good agreement with the time-domain simulations. Note that this procedure may be seen as an alternative to the REDOR transform, which provides a spectrum of the dipolar couplings for separate and isolated spin pairs [20,39]. Moreover, the
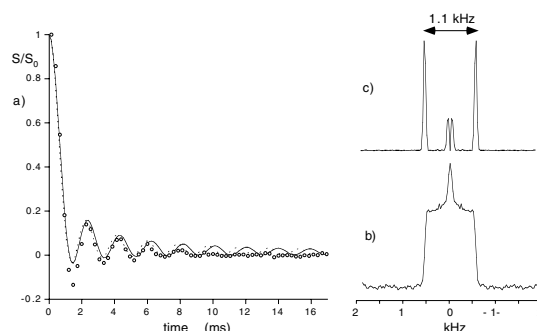


Fig. 2. REDOR data for the T-1 site of octadecasil with $\omega_r/2\pi = 15$ kHz (full MAS rotor) and $\omega_{1f}/2\pi = 49$ kHz. (**a**) REDOR dephasing signal $S/S_0$ ($\circ$) and calculations for a dipolar coupling constant $D_{IS}/2\pi = 1150$ Hz (solid line) and 1200 Hz (broken line) ; (**b**) Fourier transform of (**a**) ; (**c**) power spectrum of the derivative of (**b**).
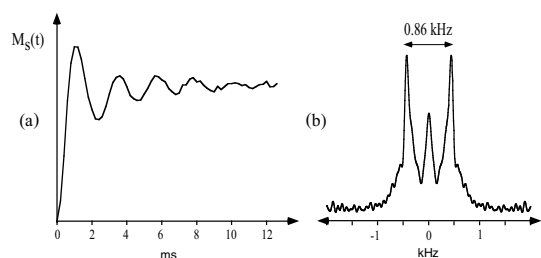
Fig. 3. The CWCP experiment in octadecasil at the $n = 1$ Hartmann–Hahn condition (T-1 site). (**a**) Time evolution at $\omega_r/2\pi = 14$ kHz using a CRAMPS rotor with $\omega_{1S}/2\pi = 20.6$ kHz and $\omega_{1I}/2\pi = 34.7$ kHz. (**b**) Fourier transformation of (**a**) after multiplication by $-1$, baseline correction and zero filling with no line broadening.

distortions in the time- and frequency-domain signals (Figs. 2a and b) are easily explained. The first negative oscillation (Fig. 2a) corresponding to intensity losses in the central region of the Pake-spun doublet (Fig. 2b) is due to the strong orientation dependence of the initial cross-polarization step at the first sideband matching condition ($n = \pm1$). Indeed, zero frequency for CP at the $n = \pm1$ condition [26] and for REDOR [12] corresponds to identical orientations of the internuclear vector in the rotor frame ($\beta = 0$ or $90°$).

Fig. 3a shows the evolution of the $^{29}$Si magnetization at the T-1 silicons in the CWCP experiment using a CRAMPS rotor for the $n = 1$ matching condition with $v_r = 14$ kHz. The heteronuclear coupling constant $D$ deduced *directly* from the line splitting $S_1$ of the Pake-like doublet obtained by Fourier transformation of the cross-polarization dynamics (Fig. 3b) leads to a Si–F distance of 2.64 Å, in excellent agreement with the X-ray determined single crystal structure and the values reported above from the REDOR experiments. The central peak is easily explained by the spin diffusion process, which is known to give rise to an additional incoherent term, corresponding to an exponential approach towards the final equilibrium state. Fortunately, for the T-1 site of octadecasil, the relevant line splitting $S_1$ is not significantly affected by this central feature (Fig. 3b). Moreover, although the RF field inhomogeneity influences the intensity of the CP signal and introduces inhomogeneous line broadening, the relevant splitting of the doublet remains unchanged [26]. Note finally that the same distance was obtained from measurements of the line splitting at the $n = 2$ Hartmann–Hahn condition, $S_2$ (data not shown). This fact further confirms the reliability of our results.
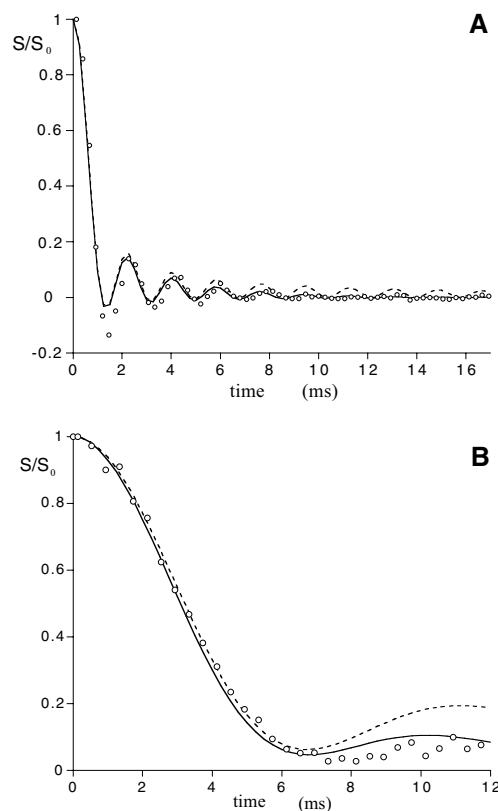


Fig. 4. Comparison of the REDOR data (○) with calculations considering all fluoride anions within a radius of 30 Å (solid line) for octadecasil with $\omega_r/2\pi = 15$ kHz. (**a**) T-1 site (same as in Fig. 3). The broken line shows the theoretical curve in the first-neighbour approximation (isolated spin pair with $r = 2.63$ Å). (**b**) T-2 site (CRAMPS rotor, $\omega_{1I}/2\pi = 75$ kHz). The broken line shows the theoretical curve for a tetrahedral arrangement with a Si–F distance of 5.69 Å.

Since the computation of $S/S_0$ can be easily generalized for an arbitrary number $n$ of spins $I$ [19,21,27], it is of interest to calculate the REDOR dephasing curve from the atomic positions of the X-ray crystal structure. This is done in Fig. 4 for both the T-1 and T-2 sites of octadecasil. We checked that the computation has converged considering all fluoride anions within a radius of 30 Å, i.e., about 200 $^{19}$F spins. For comparison, we have also plotted the signal $S/S_0$ computed for an isolated spin pair (first-neighbour approximation with $r = 2.63$ Å) in the case of the T-1 silicons (Fig. 4a) and for a tetrahedral arrangement with a Si–F distance of 5.69 Å in the case of the T-2 silicons (Fig. 4b). Clearly, the consideration of the interactions with all surrounding fluorine spins other than the first and the first four
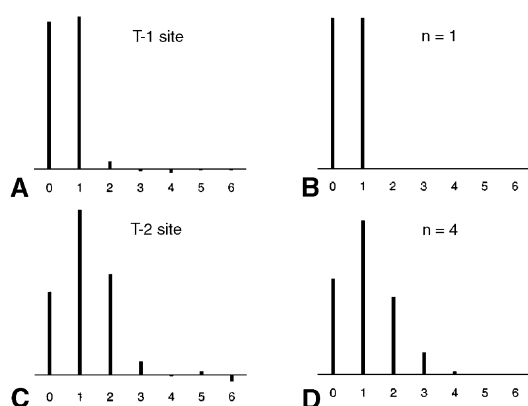
Fig. 5. Experimental and theoretical spin-counting stick spectra for the T-1 and T-2 sites of octadecasil with $\omega_r/2\pi = 15$ kHz. (**a**) Experiment for the T-1 site at the dephasing time $t_d = 6.40$ ms ($\omega_{1I}/2\pi = 50$ kHz); (**b**) theory for *SI* spin pair ($n = 1$); (**c**) experiment for the T-2 site at $t_d = 13.33$ ms ($\omega_{1I}/2\pi = 73$ kHz); (**d**) theory for a $SI_4$ spin system ($n = 4$).

fluorine neighbours of the T-1 and T-2 silicons, respectively, is equivalent to a Gaussian apodisation of the REDOR curve and improves significantly the agreement with the experimental data at long dephasing times (Fig. 4).

Our REDOR NMR results clearly confirm the X-ray crystal structure of octadecasil (Fig. 4). However, it is unclear whether reliable distances could be determined if the geometry of the spin system were completely unknown. The $\theta$-REDOR technique [20] and its generalizations [40,41] have been recently developed for measuring the $n\,S - I_k$ dipolar couplings without the additional complications arising from the orientation dependencies between the $n$ dipolar tensors. The knowledge of the spin multiplicity $n$ is nevertheless a prerequisite for extracting the coupling constants [40,41]. In this respect, it is remarked that the heteronuclear spin counting version of $\theta$-REDOR introduced by Cull et al [38] yields in principle the number $n$ of spins $I$ to which each spin $S$ is coupled. This method is based on the fact that the echo amplitude should vary as $[(1 + \cos\theta)/2]^n$ in the strong collision limit [27].

We have reported in Fig. 5 the Fourier analysis of the spin-counting $\theta$-REDOR experimental data for the T-1 and T-2 site at dephasing times $t_d = 6.40$ ms (96 rotor cycles) and 13.33 ms (200 rotor cycles), respectively. In the case of the T-1 silicon, the strong collision limit is expected to be fulfilled already at $t_d = 6.40$ ms, since Fig. 4a demonstrates that REDOR ($\theta = 180°$) dephasing is then complete (third dipolar

oscillation). The corresponding experimental stick spectrum (Fig. 5a) exhibits two peaks of almost equal amplitude at frequencies 0 and 1, the other frequency components being negligible. Hence, it is very close to the theoretical spectrum for $n = 1$ (Fig. 5b). This result fits well with the isolated Si–F spin-pair geometry at the T-1 site of octadecasil [18,25,26]. With increasing dephasing time, a significant amplitude appears at frequency 2 (data not shown). This behaviour, which is also observed in numerical simulations including all surrounding $^{19}$F spins, is readily related to the presence of additional weaker couplings, whose effect was already observed in the REDOR calculations of Fig. 4. Indeed, for $t_d > 7$ ms, Fig. 4a clearly shows that dipolar dephasing due to the multitude of surrounding fluorine spins can no longer be neglected when compared to the dominant Si–F spin pair decay. On the other hand, the Fourier analysis applied to the T-2 site shows that the spin-counting experiment with $t_d = 13.33$ ms (Fig. 5c) is best described by the $n = 4$ stick spectrum (Fig. 5d), in very good agreement with the tetrahedral environment of the $^{29}$Si nuclei in the T-2 sites (Fig. 1). However, our results show that the $\theta$-REDOR spin-counting data depend critically on the dephasing time $t_d$. Since a good estimation of $n$ has been obtained for $t_d = 6.40$ ms in the case of the T-1 site ($n = 1$) and for $t_d = 13.33$ ms in the case of the T-2 site ($n = 4$), it may be inferred that $t_d$ should be at least twice the initial magnetization decay time observed in the standard REDOR experiment (Fig. 4), but should not be much longer, in order to minimize the effect of more remote $I$ spins on REDOR dephasing. On the other hand, it is remarked that spin-counting data at longer dephasing times should give valuable information on the *local field* created by the surrounding $I$ spins.

## 5. Conclusion

$^{19}$F/$^{29}$Si Hartmann–Hahn CP and ($\theta$-)REDOR experiments can yield considerable information on molecular structure and geometry in fluoride-containing octadecasil. Reliable internuclear Si–F distances for the isolated spin pairs formed by the silicons in the D4R units and the fluoride anions can be determined from both CP and REDOR experiments under fast MAS. In fact, the CP and REDOR methods are roughly complementary in their strengths and weaknesses. In-

deed, while the CP technique, which is $\gamma$ encoded and does not require synchronization with the MAS rotation, is particularly useful in the case of relatively large dipolar interactions [26,32,33], the REDOR technique, which is well compensated for resonance offsets and rf field inhomogeneity, performs better than CP for measuring weak heteronuclear couplings [12,30]. In the case of multiple spin systems, REDOR dephasing curves are readily simulated for an arbitrary number of spins since the heteronuclear dipolar coupling Hamiltonians from various $^{19}$F spins commute with each other. Moreover, heteronuclear spin-counting $\theta$-REDOR experiments are found to be very useful to obtain direct insight into the local network of dipolar interactions. Indeed, while $^{19}$F–$^{29}$Si pair-like behaviour is confirmed at the T-1 silicon site, multiple dipolar interactions are clearly evidenced at the T-2 site.

## Acknowledgements

## References

[1] S.R. Hartmann, E.L. Hahn, Phys. Rev. 128 (1962) 2042.
[2] A. Pines, M.G. Gibby, J.S. Waugh, J. Chem. Phys. 56 (1971) 1776.
[3] A. Pines, M.G. Gibby, J.S. Waugh, J. Chem. Phys. 59 (1973) 569.
[4] J. Schaefer, E.O. Stejskal, J. Am. Chem. Soc. 98 (1976) 1031.
[5] M. Mehring, Principles of High Resolution NMR in Solids, Springer, Berlin, 1983.
[6] C.A. Fyfe, Solid State NMR for Chemists, CFC Press, Guelph, Ontario, Canada, 1983.
[7] E.O. Stejskal, J.D. Memory, High-Resolution NMR in the Solid State: Fundamentals of CP/MAS, Oxford University Press, New York, 1994.
[8] L. Müller, A. Kumar, T. Baumann, R.R. Ernst, Phys. Rev. Lett. 32 (1974) 1402.
[9] E.O. Stejskal, J. Schaefer, J.S. Waugh, J. Magn. Reson. 28 (1977) 105.
[10] B.H. Meier, Chem. Phys. Lett. 188 (1992) 201.
[11] T. Gullion, J. Schaefer, J. Magn. Reson. 81 (1989) 196.
[12] T. Gullion, J. Schaefer, Adv. Magn. Reson. 13 (1989) 57.
[13] C.P. Jaroniec, B.A. Tounge, C.M. Rienstra, J. Herzfeld, R.G. Griffin, J. Magn. Reson. 146 (2000) 132.
[14] A.W. Hing, S. Vega, J. Schaefer, J. Magn. Reson. 96 (1992) 205.
[15] G.R. Marshall, D.D. Beusen, K. Kociolek, A.S. Redlinski, M.T. Leplawy, Y. Pan, J. Schaefer, J. Am. Chem. Soc. 112 (1990) 963.
[16] S.M. Holl, G.R. Marshall, D.D. Beusen, K. Kociolek, A.S. Redlinski, M.T. Leplawy, R.A. McKay, S. Vega, J. Schaefer, J. Am. Chem. Soc. 114 (1992) 4830.
[17] A. Naito, K. Nishimura, S. Kimura, S. Tuzi, M. Aida, N. Yasuoka, H. Saitô, J. Phys. Chem. 100 (1996) 14995.
[18] C.A. Fyfe, A.R. Lewis, J.-M. Chézeau, H. Grondey, J. Am. Chem. Soc. 119 (1997) 12210.
[19] J.M. Goetz, J. Schaefer, J. Magn. Reson. 127 (1997) 147.
[20] T. Gullion, C.H. Pennington, Chem. Phys. Lett. 290 (1998) 88.
[21] E.B. Brouwer, R.D.M. Gougeon, J. Hirschinger, K.A. Udachin, R.K. Harris, J.A. Ripmeester, Phys. Chem. Chem. Phys. 1 (1999) 4043.
[22] J.C.C. Chan, H. Eckert, J. Magn. Reson. 147 (2000) 170.
[23] K. Saalwächter, H.W. Spiess, J. Chem. Phys. 114 (2001) 5707.
[24] C.P. Jaroniec, B.A. Tounge, J. Herzfeld, R.G. Griffin, J. Am. Chem. Soc. 123 (2001) 3507.
[25] C.A. Fyfe, A.R. Lewis, J.-M. Chézeau, Can. J. Chem. 77 (1999) 1984.
[26] P. Bertani, J. Raya, P. Reinheimer, R. Gougeon, L. Delmotte, J. Hirschinger, Solid State Nucl. Magn. Reson. 13 (1999) 219.
[27] P. Bertani, J. Raya, J. Hirschinger, Solid State Nucl. Magn. Reson. 22 (2002) 188.
[28] K. Schmidt-Rohr, H.W. Spiess, Multidimensional Solid-state NMR and Polymers, Academic Press, London, 1994.
[29] Y. Pan, T. Gullion, J. Schaefer, J. Magn. Reson. 90 (1990) 330.
[30] T. Gullion, Concepts Magn. Reson. 10 (1998) 277.
[31] X. Wu, K.W. Zilm, J. Magn. Reson. 104 (1993) 154 Ser. A.
[32] T. Azaïs, C. Bonhomme, L. Bonhomme-Coury, J. Vaissermann, Y. Millot, P.-P. Man, P. Bertani, J. Hirschinger, J. Livage, J. Chem. Soc., Dalton Trans. (2002) 609.
[33] T. Azaïs, L. Bonhomme-Coury, J. Vaissermann, P. Bertani, J. Hirschinger, J. Maquet, C. Bonhomme, Inorg. Chem. 41 (2002) 981.
[34] N.C. Nielsen, H. Bildsoe, H.J. Jakobsen, M.H. Levitt, J. Chem. Phys. 101 (1994) 1805.
[35] O.B. Peersen, X. Wu, S.O. Smith, J. Magn. Reson. 106 (1994) 127 Ser. A.
[36] P. Jackson, R.K. Harris, Magn. Reson. Chem. 26 (1988) 1003.
[37] A. Bax, Two-dimensional NMR in liquids, Delft University Press, Delft, 1984.
[38] T.S. Cull, J.M. Joers, T. Gullion, R.E. Norberg, M.S. Conradi, J. Magn. Reson. 133 (1998) 352.
[39] K.T. Mueller, T.P. Jarvie, D.J. Aurentz, B.W. Roberts, Chem. Phys. Lett. 242 (1995) 535.
[40] O. Liivak, D.B. Zax, J. Chem. Phys. 113 (2000) 1088.
[41] O. Liivak, D.B. Zax, J. Chem. Phys. 115 (2001) 402.